Ion Concentration Polarization in Polyelectrolyte-Modified Nanopores

ARTICLE *in* THE JOURNAL OF PHYSICAL CHEMISTRY C · APRIL 2012

Impact Factor: 4.77 · DOI: 10.1021/jp301957j

THE JOURNAL OF PHYSICAL CHEMISTRY C

Article

pubs.acs.org/JPCC

Ion Concentration Polarization in Polyelectrolyte-Modified Nanopores

Li-Hsien Yeh,[†,‡,⊥] Mingkan Zhang,[†,⊥] Shizhi Qian,[*,†,§] Jyh-Ping Hsu,[*,‡] and Shiojenn Tseng[∥]

[†]Institute of Micro/Nanotechnology, Old Dominion University, Norfolk, Virginia 23529, United States

[‡]Department of Chemical Engineering, National Taiwan University, Taipei 10617, Taiwan

[§]School of Mechanical Engineering, Yeungnam University, Gyongsan 712-749, South Korea

[∥]Department of Mathematics, Tamkang University, Tamsui, Taipei 25137, Taiwan

ABSTRACT: Nanopores functionalized with synthetic or biological polyelectrolyte (PE) brushes have significant potentials to rectify ionic current and probe single biomacromolecules. In this work, electric-field-induced ion transport and the resulting conductance in a PE-modified nanopore are theoretically studied using a continuum-based model, composed of coupled Poisson−Nernst−Planck (PNP) equations for the ionic mass transport, and Stokes and Brinkman equations for the hydrodynamic fields in the exterior and interior of the PE layer, respectively. Because of the competition between the transport of counterions and co-ions in the nanopore, two distinct types of ion concentration polarization (CP) occur at either opening of the PE-modified nanopore. These distinct CP behaviors, which significantly affect the nanopore conductance, can be easily manipulated by adjusting the bulk salt concentration and the imposed potential bias. The induced CP in the PE-modified nanopore is more appreciable than that in the corresponding bare solid-state nanopore.

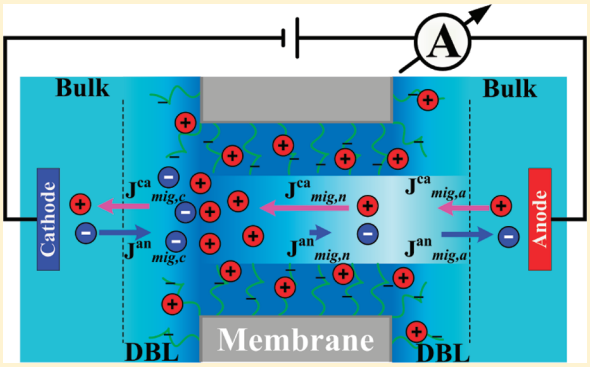

1. INTRODUCTION

Recent nanopore-based experiments strongly suggest that as the thickness of the electric double layer (EDL) becomes comparable to the characteristic length of the nanopore, several fascinating phenomena, such as ion selectivity[1,2] and ionic current rectification (ICR),[3−5] have been observed. In particular, the ion concentration polarization (CP),[5,6] induced by the selective transport of ions after the application of an electric field through a charged nanopore or nanochannel, occurs when the overlapping of EDL becomes significant. This yields an enrichment and a depletion of ion concentration regions near openings of either the nanopore or the nanochannel, known as diffusion boundary layer (DBL),[5] which in turn affects the local conductivity as well as the flow and electric fields in those regions.[7,8] With recent advances in nanofabrication techniques, a growing number of experimental results demonstrated that the presence of CP has potential applications in micro-/nanofluidics such as ICR,[9,10] electro-preconcentration of analytes,[11−13] separation of biomacromolecules,[14,15] and desalination of seawater,[16] to name a few.

Inspired by biological systems, polyelectrolyte (PE)-modified nanopores, nanometer-sized pores, or channels modified by synthetic[17−21] and biological[22−25] polymers and PEs have drawn the attention of many researchers in using them as promising platforms for sensing single biopolymers[22−24] and regulating ion transport.[17−21,25] The analysis on the ion transport in PE-modified nanopores provides necessary information for both the design of pioneering nanopore-based sensing devices and the elaboration of the physiological processes in living organisms. To date, however, relevant studies are still very limited. Recently, Tagliazucchi et al.[26] investigated the ion transport and molecular structure in polymer-modified nanopores based on a nonequilibrium molecular theory, who found that both the polymer morphology and the conductance of a nanopore are different between the low and high electric fields externally imposed.

In this study, a verified continuum-based model,[27] composed of the coupled Poisson−Nernst−Planck (PNP) equations for the ionic mass transport, and the Stokes and Brinkman equations[28,29] for the hydrodynamic fields in the exterior and interior of the PE layer, is developed for the first time to investigate the electric-field-induced ion transport and the resulting conductance in a PE-modified nanopore. This study aims to elucidate the dependence of the conductance in a PE-modified nanopore on the salt concentration and the imposed potential bias, two major parameters in nanofluidic experiments. We propose, for the first time, that the ion transport and its resulting conductance in a PE-modified nanopore involve two distinct types of counterions-rich CP occurring near either opening of the nanopore, which provide a foundation of the principles for utilizing them in practical applications.

Received: February 28, 2012
Revised: April 4, 2012
Published: April 4, 2012

   dx.doi.org/10.1021/jp301957j | J. Phys. Chem. C 2012, 116, 8672−8677

2. THEORETICAL MODEL

We consider a cylindrical nanopore of length L_N and radius R_N connecting two large, identical reservoirs on either side. The nanopore and two reservoirs are filled with an aqueous binary electrolyte solution (i.e., KCl salt solution). Polyelectrolyte (PE) chains are end-grafted to the wall surface of the membrane. For simplicity, we assume that the polyelectrolyte layer (PEL) is ion-penetrable, homogeneously structured, highly (nonregulated) charged, and of uniform thickness R_s, which yields a fixed charge density $\rho_{fix} \cong (eZ\sigma_s/R_s)$ with e, Z, and σ_s being the elementary charge, the valence of the dissociable groups per PE chain, and the surface density of PE chains grafted to the membrane, respectively. The value of σ_s typically ranges from 0.1 to 0.6 nm^{-2}.[26,30,31] Because of the symmetric nature of the present problem, we adopt the cylindrical coordinate (r, z) with the origin fixed at the center of the nanopore. A verified continuum-based model,[27,32,33] composed of the Poisson−Nernst−Planck (PNP) equations for the ionic mass transport and the modified Stokes and Brinkman equations for the liquid flow, is employed to describe the present problem.

$$-\nabla^2\phi = \frac{h\rho_{fix} + \rho_e}{\varepsilon_f} \tag{1}$$

$$\mathbf{N}_j = \mathbf{u}c_j - D_j\nabla c_j - z_j\nu_j c_j\nabla\phi \tag{2}$$

$$\nabla\cdot\mathbf{N}_j = 0 \tag{3}$$

i. PNP Equations:.[27,28,34] Here, ϕ is the electric potential; ε_f is the fluid permittivity; $\mathbf{u}$ is the fluid velocity; $\rho_e = \sum_j Fz_jc_j$ is the space charge density of the mobile ions; F is the Faraday constant; $\mathbf{N}_j$, c_j, ν_j, and z_j are the ionic flux, concentration, mobility, and valence of the jth ionic species, respectively (j = 1 for cations, and 2 for anions); and h is a unit region function (h = 0, the region outside the PEL; h = 1, the region inside it). Note that the first, second, and third terms on the right-hand side of eq 2 denote contributions from the convective, diffusive, and migrative fluxes, respectively.

ii. Modified Stokes and Brinkman Equations:.[27−29]

$$-\nabla p + \mu\nabla^2\mathbf{u} - \rho_e\nabla\phi - h\gamma\mathbf{u} = \mathbf{0} \tag{4}$$

$$\nabla\cdot\mathbf{u} = 0 \tag{5}$$

where p, μ, and γ are the hydrodynamic pressure, the fluid viscosity, and the hydrodynamic frictional coefficient of the PEL, respectively.

To specify the boundary equations associated with eqs 1−5, we assume the following: (i) The ionic concentrations at the ends of the two reservoirs are maintained at their bulk values, $c_j = C_{j0} = C_0$, and the electric potential are ϕ(cathode) = 0 and ϕ(anode) = V_0. (ii) The rigid surface of the membrane is assumed to be ion-impenetrable ($\mathbf{n}\cdot\mathbf{N}_j = 0$)[35] and uncharged ($-\mathbf{n}\cdot\nabla\phi = 0$), where $\mathbf{n}$ is the unit outer normal vector. (iii) The rigid membrane surface is nonslip ($\mathbf{u} = \mathbf{0}$), and a normal flow without external pressure gradient is assumed at the ends of the two reservoirs (p = 0). (iv) The electric field, ionic concentration, and flow field are continuous on the PEL/liquid interface.[27,29]

The conductance in the nanopore is evaluated by

$$G = I/V_0 = \int_S F(\sum_{j=1}^{2} z_j\mathbf{N}_j)\cdot\mathbf{n}dS/V_0 \tag{6}$$

where I is the ionic current, and S denotes either end of the reservoir due to the ionic current conservation.

3. RESULTS AND DISCUSSION

The strongly coupled equations, eqs 1−5, and the associated boundary conditions are numerically solved by using the commercial finite element package, COMSOL MultiPhysics (version 3.5a, www.comsol.com), operating in a high-performance cluster, which has been verified to be sufficiently efficient and accurate for solving similar electrokinetic problems.[27,36−38] The detailed description of the numerical implementation is available in our previous paper.[36]

For illustration, we consider a PE-modified nanopore with length L_N = 60 nm, radius R_N = 7 nm, and the compositions of the PEL are Z = −1 and R_s = 5 nm. The geometry of the nanopore corresponds to the typical experimental design of nanopore-based nanofluidic devices,[23,24,39,40] where the radius of the nanopore is 3−30 nm. When the radius of the nanopore is larger than 3 nm, it has been validated that the continuum-based model is still sufficient to capture and elucidate their essential physics.[41−43] In addition, the choice of the thickness of the PEL (R_s) is based on the length of the biological lipids, which typically ranges from 3 to 5 nm.[23] Because the softness degree of the PEL, $\lambda^{-1} = (\mu/\gamma)^{1/2}$,[28,29] mainly affects the hydrodynamic field inside the nanopore while the conductance is not affected significantly by the flow field,[5] we choose λ^{-1} = 1 nm, corresponding to the typical values of PEs.[28,44,45] The other physical parameters used in the simulations are $\varepsilon_f = 7.08 \times 10^{-10}$ F/m, $\mu = 1 \times 10^{-3}$ Pa·s, F = 96 490 C/mol, $\nu_1(K^+) = 7.616 \times 10^{-8}$ m^2/sV, and $\nu_2(Cl^-) = 7.909 \times 10^{-8}$ m^2/sV.

As schematically shown in Figure 1, when a potential bias V_0 is applied between the two electrodes positioned in the two

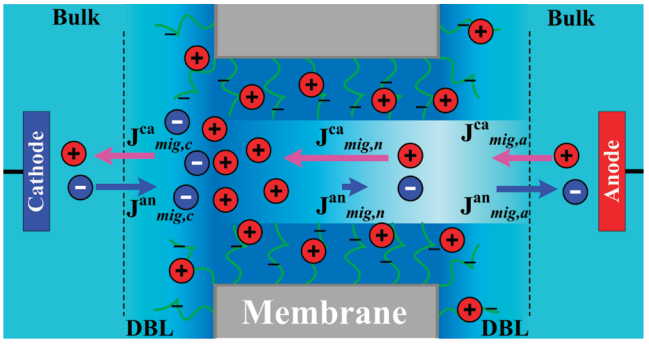

Figure 1. Schematic illustration of the CP phenomenon in a PE-modified nanopore. The superscripts "**ca**" and "**an**" denote, respectively, the migrative ionic fluxes, $\mathbf{J}_{mig}$, of the cations and anions. The migrative flux $\mathbf{J}_{mig}$ at the cathode and anode sides, and inside the nanopore, are, respectively, subscripted as *mig,c*, *mig,a*, and *mig,n*. Because $\mathbf{J}^{ca}_{mig,n}$ ($\mathbf{J}^{an}_{mig,n}$) is much larger (smaller) than $\mathbf{J}^{ca}_{mig,c}$ or $\mathbf{J}^{ca}_{mig,a}$ ($\mathbf{J}^{an}_{mig,c}$ or $\mathbf{J}^{an}_{mig,a}$), both concentrations of cations and anions are enriched at the cathode side and depleted at the anode side of the nanopore, resulting in a salt concentration gradient, the so-called diffusion boundary layer (DBL) on both openings of the nanopore.[5]

fluid reservoirs, the resulting negative axial electric field, $\mathbf{E}$, electrokinetically drives cations (anions) from the anode (cathode) side toward the cathode (anode) side and simultaneously generates a detectable ionic current through the PE-modified nanopore. Consequently, the concentration polarization (CP), arising mainly from the uneven magnitudes of the migrative fluxes of cations ($\mathbf{J}^{ca}_{mig,n}$) and anions ($\mathbf{J}^{an}_{mig,n}$)

dx.doi.org/10.1021/jp301957j | J. Phys. Chem. C 2012, 116, 8672−8677

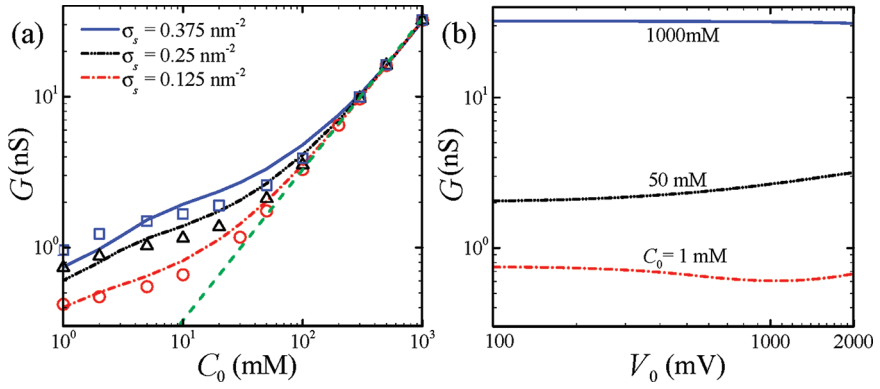

Figure 2. Conductance as a function of the bulk salt concentration C_0 at various grafting density of the PE chains on the membrane σ_s (a), and as a function of the potential bias V_0 at various C_0 when $\sigma_s = 0.25$ nm^{-2} (b). Dashed line in (a) denotes the bulk PE-modified nanopore conductance; the other lines denote the results for $V_0 = 1000$ mV. "□", "△", and "○" represent the results for $\sigma_s = 0.375$, 0.25, and 0.125 nm^{-2}, respectively, at $V_0 = 200$ mV.

inside the nanopore due to the overlapping of EDL,[5] is observed near both openings of the nanopore. As compared to the migrative flux, the contributions of the convective and diffusive fluxes are relatively small due to the low electro-osmotic flow velocity in nanofluidics[5] and low axial concentration gradient in this case. As will be shown later, we find that the migrative fluxes inside the nanopore, $\mathbf{J}^{ca}_{mig,n}$ and $\mathbf{J}^{an}_{mig,n}$, depend highly on the grafting density of the PE chains on the membrane (σ_s), bulk salt concentration (C_0), and the potential bias (V_0), which in turn induce distinct ion transport and CP phenomena as well as conductance behaviors in the PE-modified nanopore.

The influences of σ_s, C_0, and V_0 on the conductance of a PE-modified nanopore, G, are depicted in Figure 2. For comparison, the contribution of the bulk ionic concentration to the conductance of the PE-modified nanopore, $G_{bulk} \cong \pi R_N^2 F C_0(\nu_1 + \nu_2)/(L_N + 2R_s)$, is also shown by the dashed line. The other lines and symbols in Figure 2a represent the conductances for $V_0 = 1000$ and 200 mV, respectively. Figure 2a reveals that, regardless of the levels of σ_s and V_0, our results agree reasonably with the bulk conductance if C_0 is sufficiently high. Similar results can be found in Figure 2b, where G is nearly invariable when C_0 is relatively high (i.e., 1000 mM). This is expected because the overlapping of EDL is insignificant in this case,[5] and it also verifies that our numerical scheme is correct. However, for a relatively low salt concentration, the resulting G deviates appreciably from G_{bulk} and decreases nonlinearly with decreasing C_0. When C_0 is small, the overlapping of EDL inside the nanopore becomes significant, and, therefore, the fixed charges in the PEL govern the behaviors of G. In general, the amount of excess counterions accumulated inside the nanopore is proportional to σ_s (or ρ_{fix}), resulting in larger G for larger σ_s.

It is interesting to note in Figure 2a that at lower ionic concentration, the conductance G for $V_0 = 1000$ mV is larger than that for $V_0 = 200$ mV when C_0 is medium; however, when C_0 is extremely low, the conductance G at $V_0 = 1000$ mV is smaller than that at $V_0 = 200$ mV. It can be further seen in Figure 2b that the conductance G increases with increasing V_0 if C_0 is medium (i.e., 50 mM), but has a local minimum with varying V_0 if C_0 is extremely low (i.e., 1 mM). The dependence of G on C_0 and V_0 can be attributed to the ion transport in the PE-modified nanopore as illustrated in Figure 1. If C_0 is extremely low, the overlapping of EDL in the nanopore becomes very significant, resulting in more cations attracted into the nanopore, whereas anions are repelled out. After imposing voltage bias, V_0, across the nanopore, because the nanopore size is much smaller than the reservoirs, the electric field within the nanopore is much higher than that inside the reservoir. Because of the enhanced electric field and the enriched (depleted) cations (anions) inside the nanopore, the magnitude of $\mathbf{J}^{ca}_{mig,n} \gg \mathbf{J}^{an}_{mig,n}$, $\mathbf{J}^{ca}_{mig,n} \gg \mathbf{J}^{ca}_{mig,c} \cong \mathbf{J}^{ca}_{mig,a}$, and $\mathbf{J}^{an}_{mig,c} \cong \mathbf{J}^{an}_{mig,a} \gg \mathbf{J}^{an}_{mig,n}$, which leads to enriched (depleted) cations and anions at the opening of the nanopore at the cathode (anode) side. As V_0 increases, the ion transport is electrostatically hindered by the significant enrichment of ions at the cathode side of the nanopore, and, therefore, the rate of increase in $\mathbf{J}^{ca}_{mig,n}$ with increasing V_0 is less than that of increase in V_0. It can be proved in Figure 3, where the ratio of the cross-sectionally averaged migrative flux of the ionic species j ($j = 1$ for cations and $j = 2$ for anions) to the imposed potential bias, $|\overline{J}_j|/V_0$, at the cross section $z = 0$ as a function of V_0 is plotted. If C_0 is extremely low (i.e., 1 mM), $|\overline{J}_2|/V_0$ is very small and increases with increasing V_0, while $|\overline{J}_1|/V_0$ decreases with increasing V_0 until when V_0 is sufficiently large. In general, ion transport in the PE-modified nanopore takes place in the exterior region of the PEL (bright region inside the nanopore in

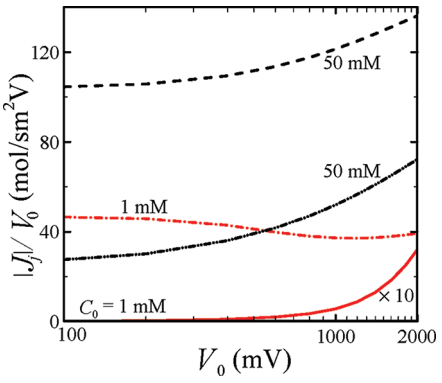

Figure 3. Ratio of the magnitude of the cross-sectionally averaged migrative flux of ionic species j ($j = 1$ for cations and $j = 2$ for anions) to the potential bias, $|\overline{J}_j|/V_0$, at $z = 0$ as a function of the potential bias. The condition is the same as that in Figure 2b. Dashed and dash-dotted lines denote $|\overline{J}_1|/V_0$; dash-double dotted and solid lines denote $|\overline{J}_2|/V_0$. A scale of 10 is applied to the solid line for clear visualization.

dx.doi.org/10.1021/jp301957j | J. Phys. Chem. C 2012, 116, 8672−8677

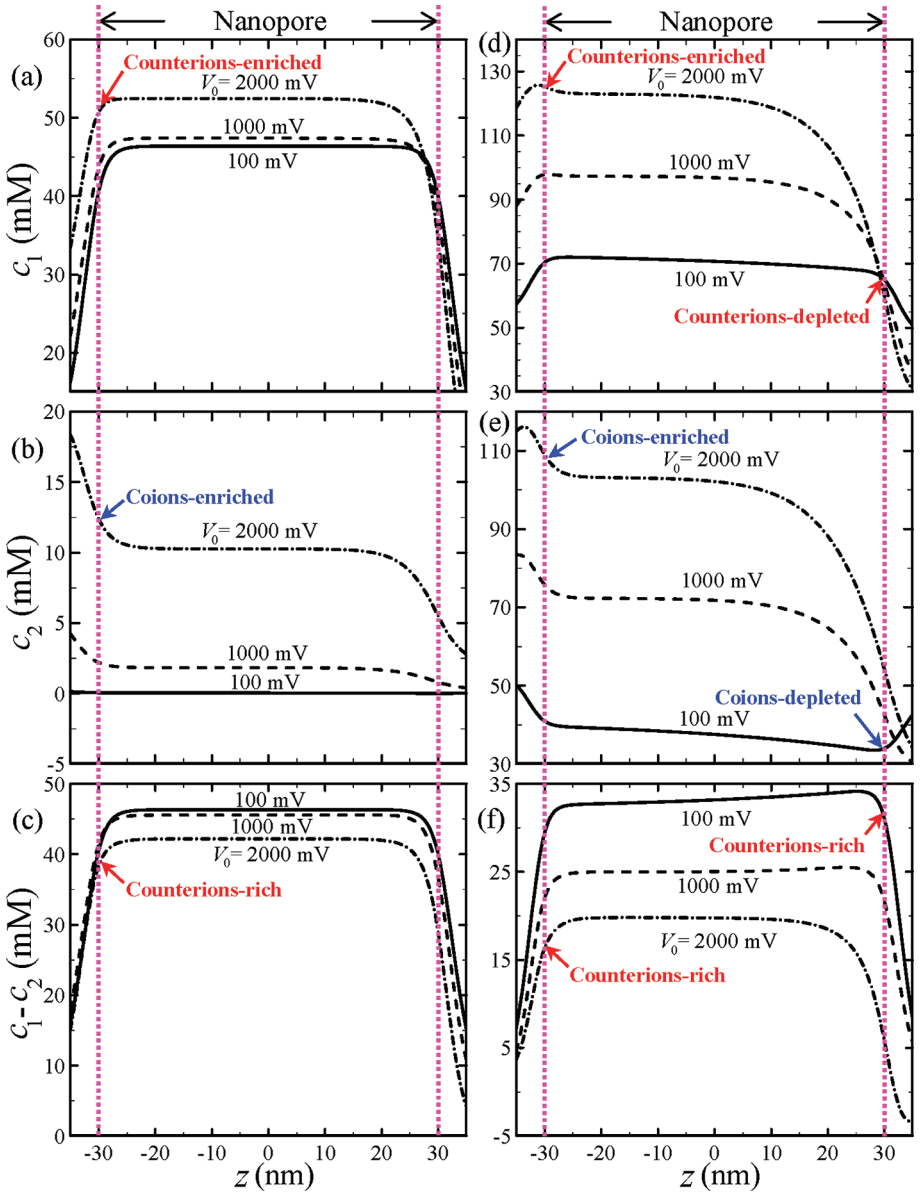

Figure 4. Concentrations of cations c_1 (a and d), anions c_2 (b and e), and the net ionic concentration difference $c_1 - c_2$ (c and f), along the axis of the PE-modified nanopore when the bulk salt concentration is C_0 = 1 mM, (a)−(c), and C_0 = 50 mM, (d)−(f), under the condition of Figure 2b. Counterions (or co-ions)-enriched represents that the concentration of counterions (or co-ions) at cathode side of the nanopore is larger than that at anode side, while counterions (or co-ions)-depleted represents that the concentration of counterions (or co-ions) at anode side of the nanopore is smaller than that at cathode side.

Figure 1) due to the highly strong equilibrium electrostatic field stemming from the charged PEL, which captures counterions inside the PEL.[28] However, if V_0 is extremely high, the strength of the applied electric field is larger than that of the equilibrium electrostatic field of the PEL, which results in the counterions (i.e., cations in the present case) inside the PEL migrating toward the cathode side of the nanopore. As a result, $|\overline{J}_1|/V_0$ shows a local minimum as varying V_0 as observed in Figure 3 (dash-dotted line). This explains the conductance behavior of the PE-modified nanopore shown in Figure 2b (dash-dotted line). On the other hand, if C_0 is higher, the overlapping of EDL becomes less significant, resulting in a larger amount of ions capable of migrating through the PE-modified nanopore as V_0 increases. As shown in Figure 3, both $|\overline{J}_1|/V_0$ and $|\overline{J}_2|/V_0$ increase as V_0 increases. This explains why the conductance increases with increasing V_0 for medium C_0 (i.e., 50 mM), as observed in Figure 2b (dash-double dotted line). It should be pointed out that the larger is the σ_s (or ρ_{fix}), the higher is amount of counterions attracted into the PE-modified nanopore, and, therefore, the hindered effect of ions becomes more significant when C_0 is low. Therefore, larger C_0 is required to induce distinct conductance behaviors with varying V_0 (cross points of lines and discrete symbols) as shown in Figure 2a.

To further understand the ion transport in the PE-modified nanopore, we plot the axial variation of the concentrations of cations, c_1, and anions, c_2, and the net ionic concentration difference, $c_1 - c_2$, in the nanopore region, as shown in Figure 4. Figure 4a−c and d−f denotes the results for C_0 = 1 and 50 mM, respectively. Because of the overlapping of EDL inside the nanopore, an enrichment (depletion) of counterions and co-ions occurs at the cathode (anode) side of the nanopore, which is the so-called CP effect as schematically illustrated in Figure 1.

dx.doi.org/10.1021/jp301957j | J. Phys. Chem. C 2012, 116, 8672−8677

Moreover, due to the competition of the ion transport through the PE-modified nanopore, there are two distinct counterions-rich CP phenomena in Figure 4. As mentioned before, if C_0 is extremely low, the overlapping of EDL is significant so that the magnitude of $J^{ca}_{mig,n} \gg J^{an}_{mig,n}$, $J^{ca}_{mig,n} \gg J^{ca}_{mig,c} \cong J^{ca}_{mig,a}$, and $J^{an}_{mig,c} \cong J^{an}_{mig,a} \gg J^{an}_{mig,n}$. Therefore, the increase of the counterions at the cathode side of the nanopore is always larger than that of the co-ions, while the reduction of the counterions at the anode side of the nanopore is always smaller than that of the co-ions. In this case, a counterions-rich CP phenomenon occurs at the cathode side of the nanopore as illustrated in Figure 4c. On the other hand, if C_0 is higher, the overlapping of EDL becomes less significant, and therefore the ion transport inside the PE-modified nanopore is not hindered significantly by the overlapping EDLs. The magnitudes of $J^{ca}_{mig,n}$ and $J^{an}_{mig,n}$ are on the same order, as shown in Figure 3, and $J^{ca}_{mig,n}$ is only slightly larger than $J^{an}_{mig,n}$. As a result, the depletion of co-ions at the opening near the anode side of the nanopore is larger than that of counterions when V_0 is small. This leads to counterions-rich CP phenomenon occurring at the anode side of the nanopore as shown in the solid line of the Figure 4d–f. However, when V_0 is large, the ions have sufficient mobilities to overcome the equilibrium electrostatic field inside the PE-modified nanopore and migrate through it. As a result, the enrichment (depletion) of the counterions (co-ions) at the cathode (anode) side of the nanopore is more significant than that of co-ions (counterions), which yields a significant counterions-rich CP phenomenon occurring at the cathode side of the nanopore as was obviously seen in the dash-dotted line of Figure 4d–f. It should be pointed out that these distinct counterions-rich CP phenomena, occurring at the opposite side of the nanopore and depending on both V_0 and C_0, have not been reported previously. In contrast, the existing studies consistently show that the counterions-rich CP only occurs at the cathode side of the nanopore.[32,46] This provides valuable information for the design of the PEs-functionalized nanofluidic devices. Wanunu et al.[47] have applied a salt concentration gradient on both sides of a solid-state nanopore to create a counterions-rich CP field, which electrostatically enhances the capture rate of DNA into the nanopore. In contrast, it is easier to induce the distinct counterions-rich CP fields by tuning the V_0 and C_0 without externally imposing the salt concentration gradient in the PE-modified nanopore.

To compare the ion concentration polarization in the present PE-modified nanopore with that in the corresponding bare solid-state nanopore, we plot the spatial distribution of the concentration difference $(c_1 - c_2)$ for both cases in Figure 5a and b, and their axial variations at various values of V_0, C_0, and σ_s in Figure 5c–e. Here, we assume that the net amount of charge in each case is the same (i.e., same σ_s). As can be seen in Figure 5a and b, because the EDL overlapping in the PE-modified nanopore is more significant than that in the corresponding solid-state nanopore, the ion CP in the former is more significant than that in the latter. Under the considered condition, the counterions-rich CP occurs on the cathode side of the nanopore. Note that the concentration of counterions (cations) is high only in the vicinity of the rigid surface of the solid-state nanopore, but remains very high outside the PEL in the PE-modified nanopore. As seen in Figure 5c–e, regardless of the levels of V_0, C_0, and σ_s, the concentration of counterions at the cathode side of the PE-modified nanopore is significantly higher than that in the corresponding solid-state nanopore. This verifies that the PE-modified nanopore is capable of creating more significant counterions-rich CP than the corresponding solid-state nanopore. Figure 5c–e also suggests that the concentration of counterions inside the PE-modified nanopore is remarkably higher than that inside the corresponding solid-state nanopore, and the difference between the two increases with increasing V_0 when σ_s is small. This is expected because the larger is the σ_s, the stronger is the equilibrium electrostatic field; therefore, a stronger applied electric field is required to induce significant ion CP. As compared to the corresponding solid-state nanopore, the PE-modified nanopore is capable of capturing more counterions and overcoming the influence of the applied electric field when the bulk salt concentration is low. These merits are advantageous to the control of the electrokinetic translocation of single biomolecules through the PE-modified nanopore.[43]

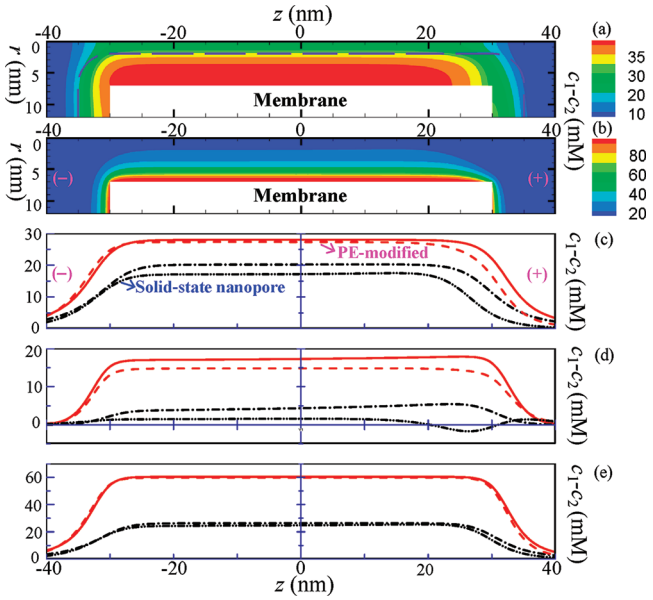

Figure 5. Spatial distribution of the net ionic concentration difference (c_1-c_2) in a PE-modified nanopore with the grafting density of the PE chains σ_s = 0.125 nm^{-2} (a) and in the corresponding solid-state nanopore with surface charge density $\sigma_w = -e\sigma_s = -20$ mC/m^2 (b) for the bulk salt concentration C_0 1 mM and the potential bias V_0 = 1000 mV. The dashed line in (a) denotes the outer boundary of the PEL. Axial variation of $(c_1 - c_2)$ in the PE-modified nanopore with σ_s = 0.125 nm^{-2} and the corresponding solid-state nanopore with $\sigma_w = -20$ mC/m^2 for C_0 = 1 mM (c) and 50 mM (d), and that in the PE-modified nanopore with σ_s = 0.375 nm^{-2} and the corresponding solid-state nanopore with $\sigma_w = -60$ mC/m^2 for C_0 = 1 mM (e). Solid (dashed) and dash-dotted (dash-double dotted) lines in (c)–(e) denote the PE-modified and solid-state nanopore at V_0 = 200 mV (V_0 = 1000 mV), respectively.

4. CONCLUSIONS

We have theoretically studied for the first time the ion transport and the resulting conductance behavior in a polyelectrolyte (PE)-modified nanopore using a continuum-based model, composed of the coupled Poisson–Nernst–Planck (PNP) equations, and Stokes and Brinkman equations. Because of the competition between the transport of ions and the equilibrium electrostatic field arising from the charged polyelectrolyte layer (PEL) in the PE-modified nanopore, two distinct counterions-rich concentration polarizations (CP), occurring at either the cathode or the anode side of the nanopore, have been found. If the bulk ionic concentration is extremely low, the counterions-

dx.doi.org/10.1021/jp301957j | J. Phys. Chem. C 2012, 116, 8672–8677

rich CP occurs at the cathode side of the nanopore, and the resulting conductance shows a local minimum with increasing strength of the imposed electric field. On the other hand, if the bulk ionic concentration is sufficiently high, the counterions-rich CP occurs at the anode side of the nanopore when the imposed electric field is relatively weak, but that occurs at the cathode side of the nanopore if the imposed electric field is relatively high. This results in the nanopore conductance increases with increasing electric field. The counterions-rich CP phenomenon occurring in the PE-modified nanopore is more significant than that in the solid-state nanopore regardless of the levels of site density of the molecular chains, the strength of the applied electric field, and the bulk ionic concentration. The results presented provide valuable information for utilizing polyelectrolyte brushes as a bridge to design the next-generation nanofluidic devices.

AUTHOR INFORMATION

Corresponding Author

*E-mail: sqian@odu.edu (S.Q.), jphsu@ntu.edu.tw (J.-P.H.).

Author Contributions

⊥These authors contributed equally.

Notes

The authors declare no competing financial interest.

ACKNOWLEDGMENTS

This work was partially supported by the World Class University Grant No. R32-2008-000-20082-0 of the Ministry of Education, Science, and Technology of Korea and the National Science Council of the Republic of China.

REFERENCES

(1) Daiguji, H. *Chem. Soc. Rev.* **2010**, *39*, 901−911.
(2) Pang, P.; He, J.; Park, J. H.; Krstic, P. S.; Lindsay, S. *ACS Nano* **2011**, *5*, 7277−7283.
(3) Cheng, L. J.; Guo, L. J. *Chem. Soc. Rev.* **2010**, *39*, 923−938.
(4) Hou, X.; Guo, W.; Jiang, L. *Chem. Soc. Rev.* **2011**, *40*, 2385−2401.
(5) Schoch, R. B.; Han, J. Y.; Renaud, P. *Rev. Mod. Phys.* **2008**, *80*, 839−883.
(6) Zangle, T. A.; Mani, A.; Santiago, J. G. *Chem. Soc. Rev.* **2010**, *39*, 1014−1035.
(7) Kim, S. J.; Wang, Y. C.; Lee, J. H.; Jang, H.; Han, J. *Phys. Rev. Lett.* **2007**, *99*, 044501.
(8) Kim, S. J.; Li, L. D.; Han, J. *Langmuir* **2009**, *25*, 7759−7765.
(9) Hlushkou, D.; Perry, J. M.; Jacobson, S. C.; Tallarek, U. *Anal. Chem.* **2012**, *84*, 267−274.
(10) Jung, J. Y.; Joshi, P.; Petrossian, L.; Thornton, T. J.; Posner, J. D. *Anal. Chem.* **2009**, *81*, 3128−3133.
(11) Wang, Y. C.; Stevens, A. L.; Han, J. Y. *Anal. Chem.* **2005**, *77*, 4293−4299.
(12) Plecis, A.; Nanteuil, C.; Haghiri-Gosnet, A. M.; Chen, Y. *Anal. Chem.* **2008**, *80*, 9542−9550.
(13) Huang, K. D.; Yang, R. J. *Electrophoresis* **2008**, *29*, 4862−4870.
(14) Inglis, D. W.; Goldys, E. M.; Calander, N. P. *Angew. Chem., Int. Ed.* **2011**, *50*, 7546−7550.
(15) Kwak, R.; Kim, S. J.; Han, J. *Anal. Chem.* **2011**, *83*, 7348−7355.
(16) Kim, S. J.; Ko, S. H.; Kang, K. H.; Han, J. *Nat. Nanotechnol.* **2010**, *5*, 297−301.
(17) Ali, M.; Ramirez, P.; Mafe, S.; Neumann, R.; Ensinger, W. *ACS Nano* **2009**, *3*, 603−608.
(18) Yameen, B.; Ali, M.; Neumann, R.; Ensinger, W.; Knoll, W.; Azzaroni, O. *Nano Lett.* **2009**, *9*, 2788−2793.
(19) Hou, X.; Liu, Y. J.; Dong, H.; Yang, F.; Li, L.; Jiang, L. *Adv. Mater.* **2010**, *22*, 2440−2443.
(20) Ali, M.; Yameen, B.; Cervera, J.; Ramirez, P.; Neumann, R.; Ensinger, W.; Knoll, W.; Azzaroni, O. *J. Am. Chem. Soc.* **2010**, *132*, 8338−8348.
(21) Actis, P.; Vilozny, B.; Seger, R. A.; Li, X.; Jejelowo, O.; Rinaudo, M.; Pourmand, N. *Langmuir* **2011**, *27*, 6528−6533.
(22) Kohli, P.; Harrell, C. C.; Cao, Z. H.; Gasparac, R.; Tan, W. H.; Martin, C. R. *Science* **2004**, *305*, 984−986.
(23) Yusko, E. C.; Johnson, J. M.; Majd, S.; Prangkio, P.; Rollings, R. C.; Li, J. L.; Yang, J.; Mayer, M. *Nat. Nanotechnol.* **2011**, *6*, 253−260.
(24) Iqbal, S. M.; Akin, D.; Bashir, R. *Nat. Nanotechnol.* **2007**, *2*, 243−248.
(25) Ali, M.; Neumann, R.; Ensinger, W. *ACS Nano* **2010**, *4*, 7267−7274.
(26) Tagliazucchi, M.; Rabin, Y.; Szleifer, I. *J. Am. Chem. Soc.* **2011**, *133*, 17753−17763.
(27) Zhang, M. K.; Yeh, L. H.; Qian, S.; Hsu, J. P.; Joo, S. W. *J. Phys. Chem. C* **2012**, *116*, 4793.
(28) Yeh, L. H.; Hsu, J. P. *Soft Matter* **2011**, *7*, 396−411.
(29) Ohshima, H. *Adv. Colloid Interface Sci.* **1995**, *62*, 189−235.
(30) Peleg, O.; Tagliazucchi, M.; Kroger, M.; Rabin, Y.; Szleifer, I. *ACS Nano* **2011**, *5*, 4737−4747.
(31) Marsh, D.; Bartucci, R.; Sportelli, L. *Biochim. Biophys. Acta, Biomembr.* **2003**, *1615*, 33−59.
(32) Vlassiouk, I.; Smirnov, S.; Siwy, Z. *Nano Lett.* **2008**, *8*, 1978−1985.
(33) Liu, H.; Qian, S. Z.; Bau, H. H. *Biophys. J.* **2007**, *92*, 1164−1177.
(34) Zhang, M. K.; Ai, Y.; Kim, D. S.; Jeong, J. H.; Joo, S. W.; Qian, S. Z. *Colloids Surf., B* **2011**, *88*, 165−174.
(35) Ai, Y.; Liu, J.; Zhang, B. K.; Qian, S. *Anal. Chem.* **2010**, *82*, 8217−8225.
(36) Ai, Y.; Zhang, M. K.; Joo, S. W.; Cheney, M. A.; Qian, S. Z. *J. Phys. Chem. C* **2010**, *114*, 3883−3890.
(37) Zhang, B. K.; Ai, Y.; Liu, J.; Joo, S. W.; Qian, S. Z. *J. Phys. Chem. C* **2011**, *115*, 24951−24959.
(38) Ai, Y.; Liu, J.; Zhang, B. K.; Qian, S. Z. *Sens. Actuators, B* **2011**, *157*, 742−751.
(39) Chang, H.; Kosari, F.; Andreadakis, G.; Alam, M. A.; Vasmatzis, G.; Bashir, R. *Nano Lett.* **2004**, *4*, 1551−1556.
(40) Hou, X.; Yang, F.; Li, L.; Song, Y. L.; Jiang, L.; Zhu, D. B. *J. Am. Chem. Soc.* **2010**, *132*, 11736−11742.
(41) van Dorp, S.; Keyser, U. F.; Dekker, N. H.; Dekker, C.; Lemay, S. G. *Nat. Phys.* **2009**, *5*, 347−351.
(42) He, Y. H.; Tsutsui, M.; Fan, C.; Taniguchi, M.; Kawai, T. *ACS Nano* **2011**, *5*, 5509−5518.
(43) Yeh, L. H.; Zhang, M. K.; Qian, S.; Hsu, J. P. *Nanoscale* **2012**, *4*, 2685−2693.
(44) Yeh, L. H.; Liu, K. L.; Hsu, J. P. *J. Phys. Chem. C* **2012**, *116*, 367−373.
(45) Duval, J. F. L.; Gaboriaud, F. *Curr. Opin. Colloid Interface Sci.* **2010**, *15*, 184−195.
(46) Choi, Y. S.; Kim, S. J. *J. Colloid Interface Sci.* **2009**, *333*, 672−678.
(47) Wanunu, M.; Morrison, W.; Rabin, Y.; Grosberg, A. Y.; Meller, A. *Nat. Nanotechnol.* **2010**, *5*, 160−165.